

Convective Systems Developed along the Coastline of Sumatera Island, Indonesia, Observed with an X-band Doppler Radar during the HARIMAU2006 Campaign

Shuichi MORI, HAMADA Jun-Ichi

*Research Institute for Global Change (RIGC),
Japan Agency for Marine-earth Science and Technology (JAMSTEC), Yokosuka, Japan*

Namiko SAKURAI

National Research Institute for Earth Science and Disaster Prevention (NIED), Tsukuba, Japan

Hironori FUDEYASU

Yokohama National University, Yokohama, Japan

Masayuki KAWASHIMA

Institute for Low Temperature Science, Hokkaido University, Sapporo, Japan

Hiroyuki HASHIGUCHI

Research Institute for Sustainable Humanosphere, Kyoto University, Kyoto, Japan

Fadli SYAMSUDIN, Ardhi A. ARBAIN, Reni SULISTYOWATI

Agency for the Assessment and Application of Technology (BPPT), Jakarta, Indonesia

Jun MATSUMOTO

*Research Institute for Global Change (RIGC),
Japan Agency for Marine-earth Science and Technology (JAMSTEC), Yokosuka, Japan
Department of Geography, Tokyo Metropolitan University, Hachioji, Japan*

and

Manabu D. YAMANAKA

*Research Institute for Global Change (RIGC),
Japan Agency for Marine-earth Science and Technology (JAMSTEC), Yokosuka, Japan
Graduate School of Science, Kobe University, Kobe, Japan*

(Manuscript received 30 April 2010, in final form 28 September 2010)

Corresponding author: Shuichi Mori, Research Institute for Global Change (RIGC), Japan Agency for Marine-Earth Science and Technology (JAMSTEC), 2-15 Natsushima-cho, Yokosuka, Kanagawa 237-0061, Japan.
E-mail: morishu@jamstec.go.jp
© 2011, Meteorological Society of Japan

Abstract

An overview of convective activity during the HARIMAU2006 campaign conducted from 26 October to 27 November 2006 was presented, focusing on the differences between coastal land/sea and inactive/active phases of intraseasonal variation (ISV) based on observations using an X-band Doppler radar (XDR) and intensive soundings at Sumatera Island. Diurnal variation (DV) in coastal convections and formation of the coastal heavy rainband (CHeR) along Sumatera Island were also examined in terms of diurnal land-sea migration of coastal convective systems.

Convection in the ISV inactive period (PP1) contained convective rain fractions nearly twice as much as stratiform rain fractions, whereas that in the ISV active period (PP2) comprised convective and stratiform elements almost equally. Vertical profiles of radar echo coverage for stratiform rain during PP2 were greater than those during PP1, especially in the lower troposphere over the sea. The radar echo coverage for convective rain over the sea during both periods was nearly double that over land from the near surface up to 6 km high.

Convection was generated in the southwestern foothills of the mountain range in the early afternoon (12–15 Local Time, LT). Part of the convective system remained over the coastal land and exhibited weak reflectivity until the next morning. The other part migrated offshore at a speed of approximately 4 m s^{-1} and intensified until around 21 LT while still offshore. Additional convective cells also developed offshore in the early morning hours, independent of those that formed over land. Results suggested that the CHeR along Sumatera Island is dictated by diurnal variations in coastal convective development and consists of the following phases: 1) migration of convection away from the coastal land and its redevelopment in the late evening, and 2) additional generation of convection just offshore during the early morning hours.

1. Introduction

Coastal regions over the tropics exhibit unique characteristics in terms of their convective activity. Heavy rainbands tend to form along coastlines, and the rainfall variation has a strong diurnal component.

Xie et al. (2006) showed several heavy rainbands that developed in the boreal summer season along coastlines over the Asian monsoon region. These rainbands were identified using long-term observations from the Tropical Rainfall Measuring Mission (TRMM) satellite. They identified rainbands along the Indian coast west of the Western Ghats, the western coast of Myanmar over the Bay of Bengal and the Andaman Sea, northeastern coast of the Gulf of Thailand, the eastern coast of Vietnam, and the northwestern Philippines. They showed that rainfall distribution in the tropics is not uniform, but instead is anchored by mountains along these coastlines that cause a wind-terrain interaction during the boreal summer monsoon season. Though it was not mentioned by Xie et al. (2006), a heavy rainband was also identified along the southwestern coastline of Sumatera Island in the Indonesian maritime continent (IMC). This rainband was found in the boreal summer season, but its effect was also noted in the long-term annual mean rainfall (Mori et al. 2004).

Diurnal variation (DV) is widely known to be one of the most dominant modes of convective activity in the tropics (e.g., Nitta and Sekine 1994; Ohsawa et al. 2001). Intraseasonal variation (ISV), including the Madden-Julian oscillation (MJO), is also an essential mode of convective activity in the tropics (Madden and Julian 1971, 1972). In general, rainfall DV is characterized by evening (morning) rain over land (sea) due to the different heat capacities of the two surfaces and related local land-sea circulations (Johnson et al. 2001; Tao et al. 1996; Sui et al. 1998; Zhou and Wang 2006). As a result, coastlines exhibit contrasts between evening and morning rainfall over the coastal land and sea, respectively, and produce unique characteristics of convection in those regions. In fact, Mori et al. (2004) showed clear contrast between the evening (12–23 Local Time, LT) and morning (00–11 LT) rain along the coastlines of major islands of the IMC, such as Sumatera, Kalimantan, Jawa, Sulawesi, and Papua Islands, using data from the precipitation radar (PR) on the TRMM satellite. In addition, they showed that the peak time of rainfall DV is delayed according to the distance both for inland and offshore sides from the coastline. Similar phase delays of rainfall DV are widely seen along coastlines in the tropics such as the southeastern coast of the Bay of Bengal (Zuidema 2003), the northwestern coast of South America (Mapes et al.

2003), and the northern coast of Papua (Moteki et al. 2008). This suggests that coastlines play an important role in the control of convective DV in the tropics.

Most coastal rainfall patches (or coastal heavy rainbands, CHeRs) are concentrated just offshore, and not on land (Xie et al. 2006). This cannot be explained solely in terms of the wind-terrain interaction (Ogura and Yoshizaki 1988). Recently, Wu et al. (2009) and Hara et al. (2009) also noted that the coastal heavy rainband along Sumatera Island was not well simulated. Even in high-resolution general circulation models (GCMs), the rainband was reproduced over the coastal land but not in the nearshore region. They suggested that problems with GCMs that cannot simulate convective DV well (e.g., Yang and Slingo 2001; Neal and Slingo 2003) may have caused these errors.

Rainfall levels over the IMC are among the highest globally. Spatial and temporal variations in rainfall affect the global circulation through latent heat release (Ramage 1968). Because the IMC is composed of a large number of islands and surrounding sea, both regional and temporal variations in rainfall may be quite complicated due to strong interactions between land and adjacent sea through their heterogeneous radiation properties and local circulations. Convective activity over the IMC has been studied using satellite, objective analysis, and daily and/or monthly rainfall data in terms of diurnal (Hamada et al. 2008; Qian 2008; Sakurai et al. 2005; Yang and Slingo 2001), intra-seasonal (Hamada et al. 2008; Nitta et al. 1992; Ichikawa and Yasunari 2008), seasonal (Hamada et al. 2002; Matsumoto 1992; Tanaka 1994; Murakami and Matsumoto 1994), and interannual variations (Hamada et al. 2002; Yasunari 1981). However, due to the limited frequency of operational rawinsonde observations in Indonesia (Okamoto et al. 2003), sounding data and their related products such as the objective analysis data over the IMC cannot resolve the DV in atmospheric structures. It is widely known that data from infrared (IR) sensors on geostationary satellites show several hours of phase delay in the peak time of convective DV in comparison with *in situ* surface rainfall observations because IR sensors detect cloud top temperature (Houze et al. 1981; Ohsawa et al. 2001; Kubota and Nitta 2001). Though TRMM PR can resolve the rainfall DV correctly with enough spatial and temporal resolutions over the globe (Hirose and Nakamura 2005; Hirose et al. 2008), it cannot

capture the evolution and decay processes of convection embedded in the DV owing to its low sampling frequency over the equatorial tropics. Moreover, the hierarchical structure of mesoscale convective systems (MCSs) especially over coastal regions and their interaction with synoptic disturbances, including the ISV and/or monsoon, have not been closely analyzed in previous studies because of the coarse spatial and temporal resolutions of the data in those studies; nevertheless, such studies are crucial to the discussion of the formation of CHeRs over the IMC.

Recently, campaign observations of Coupled Processes in the Equatorial Atmosphere (CPEA) have been conducted over the mountainous region of Sumatera Island (Fukao 2006). The structure and dynamics of convective cells have been studied in detail using an X-band Doppler radar (XDR), Equatorial Atmosphere Radar (EAR) and intensive soundings (Kawashima et al. 2006; Mori et al. 2006; Sakurai et al. 2009a; Shibagaki et al. 2006). However, convection over the southwestern coastal region of the island, which is an essential region for our study, was not covered by the XDR because of the complicated high topography around the XDR and EAR.

Coastal regions in the tropics, especially in Asian monsoon countries including the IMC, have high populations and significant industrial activity. A small difference in the location of CHeRs over land or the sea can greatly affect local communities (e.g., through natural disasters and/or changes in agriculture/water resource management). In addition, this convection can sometimes generate hazardous windstorms in the foothills of mountain ranges along the coast (Kawashima et al. 2011). Therefore, it is important to increase our understanding of the physical processes related to the DV in convective activity in these regions for scientific and practical reasons.

For this reason, we performed the first campaign observation of Hydrometeorological ARray for ISV-Monsoon AUtomonitoring (HARIMAU; Yamanaka et al. 2008), called "HARIMAU2006", to investigate the characteristics of convective activity along the southwestern coastline of Sumatera Island and their interaction with the ISV, mainly using two XDRs and intensive atmospheric soundings from 26 October to 27 November 2006. This paper presents an overview of convective activity during the HARIMAU2006, focusing on the differences between coastal land/sea and inactive/active

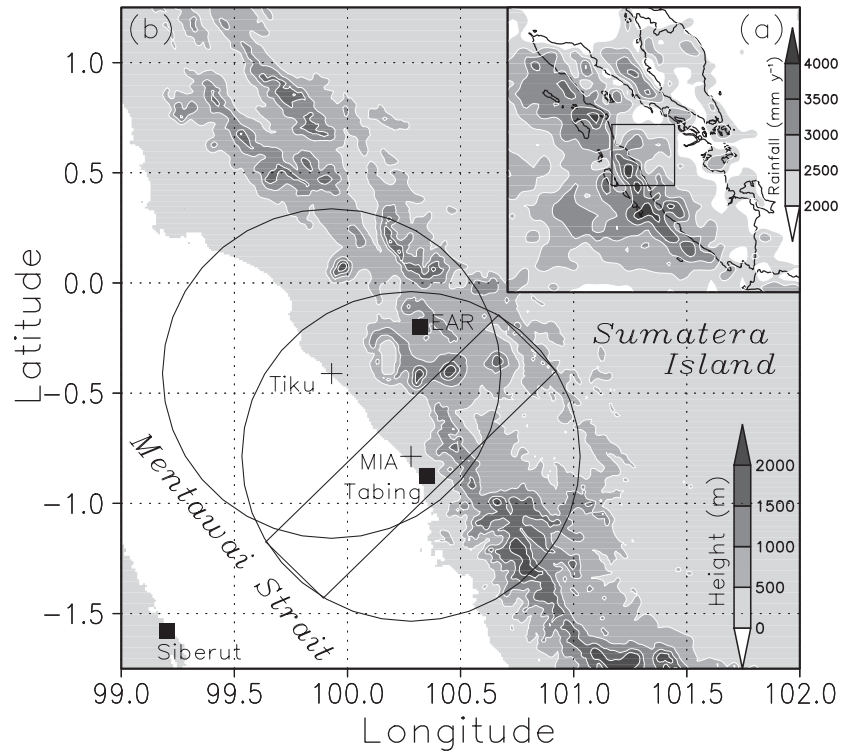


Fig. 1. (a) Averaged annual rainfall over Sumatera Island, Indonesia, observed with TRMM PR during 1998–2006. A small square corresponds to an area of panel (b).

(b) Locations of two X-band Doppler radars (XDRs; MIA and Tiku), rawinsonde stations (Tabing and Siberut), and Equatorial Atmosphere Radar (EAR) in west Sumatera Island with topography. The two circles show maximum ranges (83 km) of observation from the two XDRs, and the rectangle depicted in the range of MIA-XDR is an area of analysis in Section 3. Elevation contours are depicted every 500 m.

ISV phases based on observations with the XDR and intensive soundings at Sumatera Island. In addition, the DV in coastal convection and formation of CHeR are also examined in terms of diurnal land-sea migration of coastal convection.

The HARIMAU2006 was performed in collaboration with the *Mirai* Indian Ocean cruise for the Study of the MJO-convection Onset (MISMO) project (Yoneyama et al. 2008). The MISMO deployed the R/V *Mirai* over the Indian Ocean (80.5°E, EQ) and observatories at Gan Island (73.2°E, 0.7°S) and other islands of Maldives to investigate zonal structure and evolution of the first MJO onset using Doppler radars and intensive soundings at multiple locations. We aimed to obtain simultaneous observational data to examine them at the eastern end of Indian Ocean though the HARIMAU2006, however, it was out of scope in this study.

2. Observation and data

2.1 Framework

We conducted the HARIMAU2006 campaign between 26 October and 27 November 2006 (33 days) in the major rainy season over the west Sumatera Island. Figure 1a shows a 10-year map (1998–2007) of average annual rainfall pattern over Sumatera Island obtained from the TRMM PR. Rainfall greater than 3,000 mm y^{-1} was observed along the southwestern coast of the island. The CHeR was located over the sea, not over land. The small rectangle inside the figure corresponds to Fig. 1b, which shows the allocation of XDRs and sounding stations along the coast with topographical elevation.

Two XDRs were installed at Minangkabau International Airport (MIA; 0.79°S, 100.30°E, 5 m above mean sea level, AMSL) and Tiku (0.40°S,

99.92°E, 3 m AMSL) to observe the behavior of convection over both the coastal land and sea. In addition, intensive soundings in 3–6 hour intervals were conducted at Tabing (0.88°S, 100.35°E, 3 m AMSL) and at Siberut (1.58°S, 99.20°E, 7 m AMSL) on both sides of the Mentawai Strait to obtain the atmospheric structure over sub-diurnal temporal scales. Surface meteorological data were obtained at those observatories by automatic weather stations (AWSs). Moreover, rainwater was sampled at high temporal resolution at both Tabing and Siberut for stable isotope analysis (Fudeyasu et al. 2011).

2.2 Doppler radars

We deployed two XDRs at the MIA and Tiku sites, which operated continuously from 26 October to 27 November 2006. The major specifications of the XDRs are summarized in Table 1. The XDRs obtained three-dimensional reflectivity and Doppler velocities every 6 min through a series of conical scans with antenna elevation from 0.5° to 50° at both stations. The observation radii of both XDRs were 83 km, as shown in Fig. 1b. In addition, the XDR at MIA made surveillance observations at one elevation angle (0.5°) with a radius of 166 km every 6 min. The reflectivity and radial Doppler velocity were interpolated over Cartesian coordinates with grid intervals of 0.5 km (333 × 333 grids in a 166 × 166 km square) in the horizontal and 0.5 km in the vertical (40 levels from 0.5 to 20 km AMSL) plane.

Reflectivity fields were partitioned into convective and stratiform regions by using a technique proposed by Steiner et al. (1995) because the two rainfall types have crucial differences in their latent heat profiles (Houze 1982) and affect the surrounding atmosphere differently. We calculated the hourly rainfall rates from the reflectivity field using Z-R relations for each rainfall type, where Z and R are radar reflectivity and rainfall rate, respectively. In this study, we employed the Z-R relations as first-guess values for rainfall rate estimation in the TRMM 2A25 version 5 algorithm, i.e., $Z = 148 R^{1.55}$ for convective rainfall, $Z = 276 R^{1.49}$ for stratiform rainfall (Schumacher and Houze 2003), to facilitate comparison of the rainfall characteristics among various regions. Then, the rainfall rates were averaged over the maximum volume-scan coverage area.

We used the radar echo coverage (%) observed by the XDR only at MIA in the following analyses.

Table 1. Major specifications of MIA and Tiku XDRs and their operating condition during the HARI-MAU2006 campaign.

Parameter	Value	
Radar site	MIA	Tiku
Location	0.79°S, 100.30°E 5 m AMSL	0.40°S, 99.92°E 3 m AMSL
Manufacture	Japan Radio Company Ltd. (JRC)	
Frequency	9770 MHz	9445 MHz
Peak power	70 kW	40 kW
Pulse width	0.5 μs	
PRF	1800 Hz	
	Dual PRF [600/ 900 Hz] for PPI surveillance mode	—
Beam width	0.98 deg	1.1 deg
Signal processor	RVP8	RVP7
	Sigmet Product Line	
Maximum range	83 km	
	160 km for PPI surveillance mode	—
Sampling space	200 m	
Antenna rotation speed	30 deg sec ⁻¹	
Elevation angles	0.5 to 50.0 deg	
	18 elevations	19 elevations
Nyquist velocity	13.8 m s ⁻¹	16 m s ⁻¹
Time interval	Every 6 min	

Because the XDR at Tiku frequently experienced stoppages due to electrical power supply problems, it could not obtain enough data during the whole period; however it was utilized for dual Doppler radar analyses and other case studies (Kawashima et al. 2011). Radar echo coverage was defined as the area of radar echo (km²) with a radar reflectivity of more than 10 dBZ at a specific height divided by an area of radar detection (km²) at the same height. Because of the complicated topography (Fig. 1b), the radar detection area over the

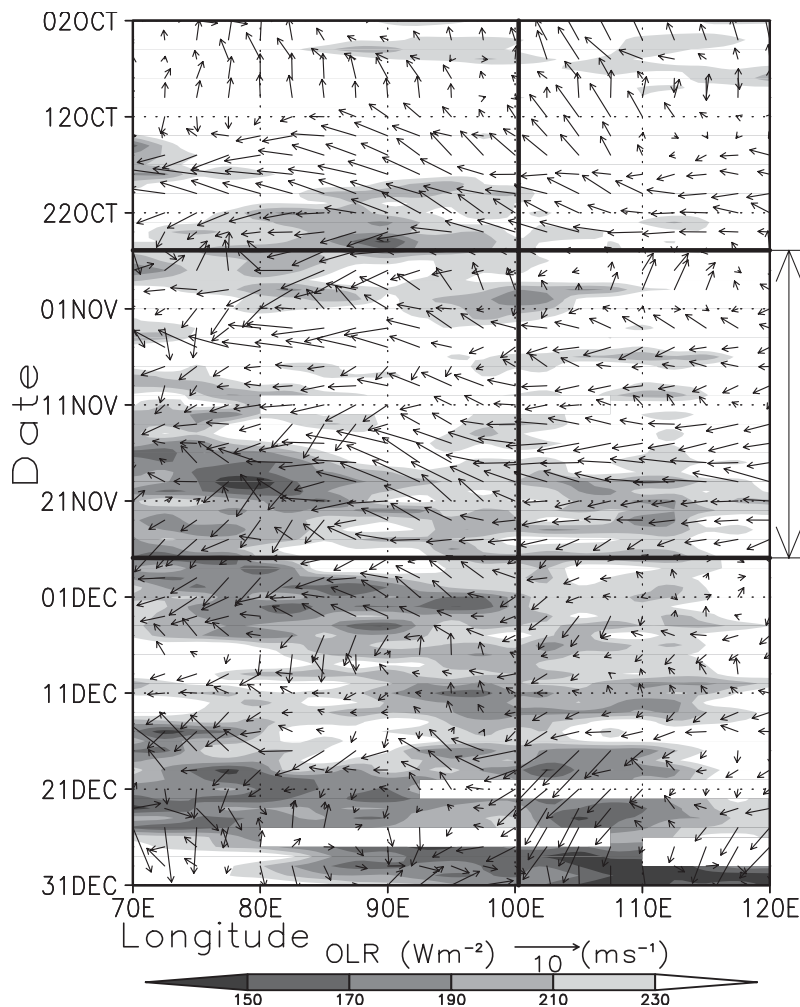


Fig. 2. Hovmöller diagram of OLR with NCEP wind vectors at 850 hPa averaged over the latitude of 5°S–5°N from 02 October to 31 December 2006. The vertical solid line near 100°E shows the location of the MIA-XDR site. The date between two horizontal thick lines (26 October–27 November 2006) indicates the HARIMAU2006 campaign period.

land varied greatly, particularly below 2 km AMSL (figure not shown).

2.3 Intensive soundings

Rawinsondes (Vaisala RS-92SGP) were launched at Tabing over the whole observation period of 26 October to 27 November 2006 and at Siberut during 3–15 November 2006. We took soundings four times a day (00, 06, 12, and 18 UTC) at both sites and took additional soundings at four other times (03, 09, 15, and 21 UTC) during 4–14, 25, and 26 November 2006 at Tabing, and 9–13 November 2006 at Siberut. All soundings provided vertical profiles of pressure, temperature, relative

humidity, and horizontal wind every 2 seconds, which corresponded to a height resolution of approximately 10 m. Sounding data from Tabing averaged vertically every 100 m were used in the following analyses.

2.4 Surface observations

AWSs (Vaisala MAWS201) were deployed at MIA, Tiku, Tabing, and Siberut. They provided surface pressure, temperature, relative humidity, solar radiation, wind direction and speed, and rainfall. The minimum sensitivity for the rainfall amount and the temporal resolution of the recorded data were 0.5 mm and 10 min at Tabing

(Ogasawara RS-102 rain gauge), and 0.2 mm and 1 min at the other stations (Vaisala QMR101 rain gauges). AWS data observed only at MIA were used in the following analyses.

2.5 Other data

TRMM PR 10-year (1998–2007) precipitation data based on the monthly 3A25 dataset provided by the Japan Aerospace Exploration Agency (JAXA) were used to examine the climatology of the CH_{ER} along the southwestern coastline of Sumatera Island. Both outgoing longwave radiation (OLR) and objective reanalysis data provided by the National Oceanic and Atmospheric Administration (NOAA) and National Centers for Environmental Prediction (NCEP), respectively, were used to analyze large-scale convective activity and related circulation during this period. The spatial and temporal resolutions of both datasets were 2.5×2.5 degrees and 1 day, respectively. An all-season real-time multivariate MJO index (RMM) provided by the Bureau of the Meteorology Research Centre (BMRC) was also used to confirm the phases of the MJO activity during this period. In addition, the GTOPO30 global digital elevation model (DEM) dataset provided by the U.S. Geological Survey (USGS) with a spatial resolution of 30-min arcseconds was used to confirm the area of radar detection and depict the topography around the study region.

3. Results

3.1 Large-scale conditions during the study period

The HARIMAU2006 was originally designed to observe coastal convective activity during the first MJO onset in collaboration with the MISMO. Hence, it was set in the boreal autumn season (one month from late October to late November). A Hovmöller diagram of OLR and wind vectors at 850 hPa from October to December 2006 is shown in Fig. 2 to confirm synoptic convective activity and circulations from the western Indian Ocean to Sumatera Island (5°S – 5°N). Low OLR regions correspond to large-scale disturbances that appeared in the middle of the Indian Ocean (70° – 80°E) around 10 November and approached Sumatera Island (100°E) after 15 November. More active convective regions with much smaller OLR arrived at the island after the middle of December. However, the OLR was generally high, and large-scale convection was inactive around the island before the middle of November. Wind in the lower troposphere

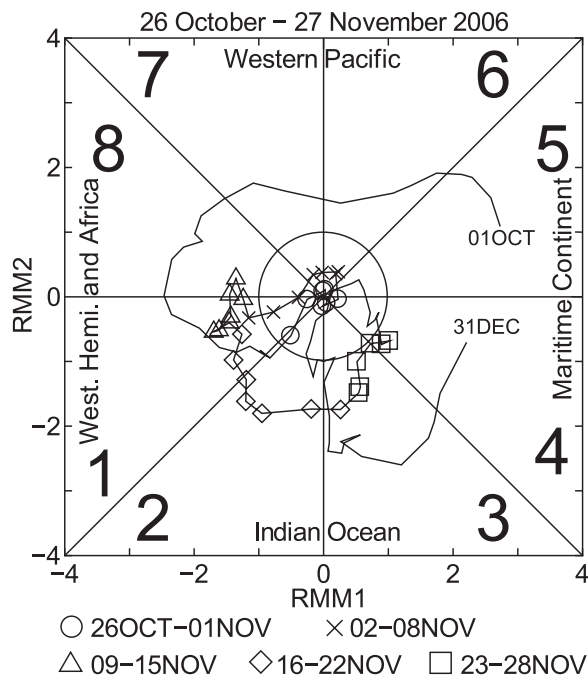


Fig. 3. All-season real-time multivariate MJO index (RMM) during 01 October to 31 December 2006. The index during the HARIMAU2006 campaign period was divided in 5 terms (each 7 days, except the last term) denoted by each mark.

during the campaign period was easterly in general, but it was weaker after the large-scale disturbance approached the island.

The large-scale disturbance after the middle of November shown in Fig. 2 was diagnosed as a MJO based on the RMM chart (Fig. 3). The MJO signal started at the maritime continent sector (RMM 5) from 01 October and then propagated eastward. Although it became stagnant once just before the Indian Ocean by 26 October and 17 November, it started to propagate eastward again over the Indian Ocean sector (RMM 2–3) smoothly. Because it approached the western tip of the maritime continent sector (RMM 4) at the end of 23–28 November, we assume that Sumatera Island was located at the leading edge of the MJO active convective region in the last quarter of the campaign period. Indeed, because the average specific humidity at 850 hPa averaged from October to November 2006 (Fig. 4) was concentrated over the eastern Indian Ocean and the west of Sumatera Island, the atmosphere in the lower troposphere was wet enough

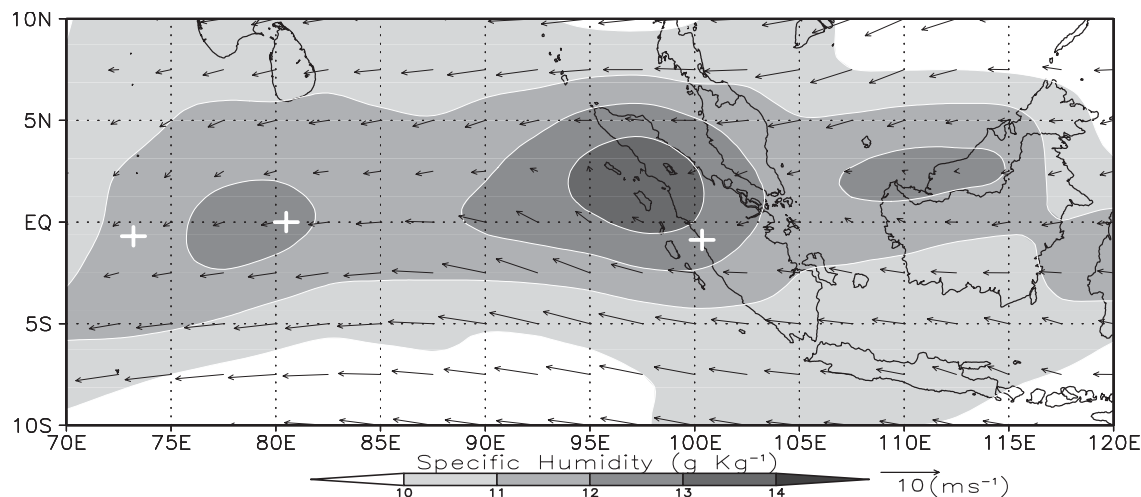


Fig. 4. Horizontal fields of specific humidity and wind vectors at 850 hPa obtained by NCEP reanalysis over the eastern Indian Ocean and western part of Indonesian maritime continent averaged for the HARIMAU2006 campaign period (26 October–27 November 2006). White crosses indicate sounding stations at Tabin (0.88°S , 100.35°E) in Sumatera Island, R/V Mirai (EQ, 80.5°E), and Gan Island in the Maldives (0.7°S , 73.2°E).

to generate convection, even though it was mainly in the MJO inactive phase.

Yoneyama et al. (2008) examined the same large-scale disturbances during the same period and identified that this disturbance, which passed over Sumatera Island during the HARIMAU2006, was not exactly caused by the MJO by their analysis based on Wheeler and Weickmann (2001), although it showed intraseasonal variability. Therefore, in the following analyses, we refer to the large-scale disturbance shown during the campaign period as the ISV.

3.2 Local weather conditions

We examined the day-to-day variation in sounding and area-averaged rainfall data to identify the local weather conditions during the HARIMAU2006. Figure 5 shows time-height cross sections of (a) equivalent potential temperature, (b) specific humidity, (c) zonal and (d) meridional wind speeds observed by intensive sounding from 26 October to 27 November 2006 at Tabin (Fig. 1). Potential equivalent temperature and specific humidity are shown as anomalies from the period mean at each height.

Easterly wind appeared in the troposphere during the whole period, as can be seen from the synoptic conditions (Figs. 2 and 4), although the weak westerly wind was generally the dominant climatol-

ogy below 5 km in this period (Okamoto et al. 2003). The easterly wind speed below 10 km decreased, and westerly wind appeared in the beginning (26–31 October), middle (10–15 November), and end (23–27 November) of the period. An apparent westerly wind was observed below 1 km almost every day, which corresponded to the sea breeze circulation across the northwest-southeast oriented coastline (Fig. 1b). The meridional wind showed clear 4–5 day variation below 10 km, with upward propagation that may have been related to the mixed Rossby-gravity wave because disturbances with similar periods propagated westward with small zonal wind components (Kawashima et al. 2010). Similar to the zonal wind variation, there was southerly wind flow almost continuously below 1 km, which had a component of sea breeze circulation, but did not show clear diurnal alternation.

Both the equivalent potential temperature and specific humidity clearly showed diurnal variations from the near surface to the middle or even approaching the tropopause. Both quantities were large when the zonal wind was weak easterly or westerly in the beginning, middle, and last parts of the period mentioned above. They were largest in the lower troposphere during the last 6 days (22–27 November 2006), when the large-scale disturbance approached Sumatera Island as starting the ISV active phase (Fig. 2).

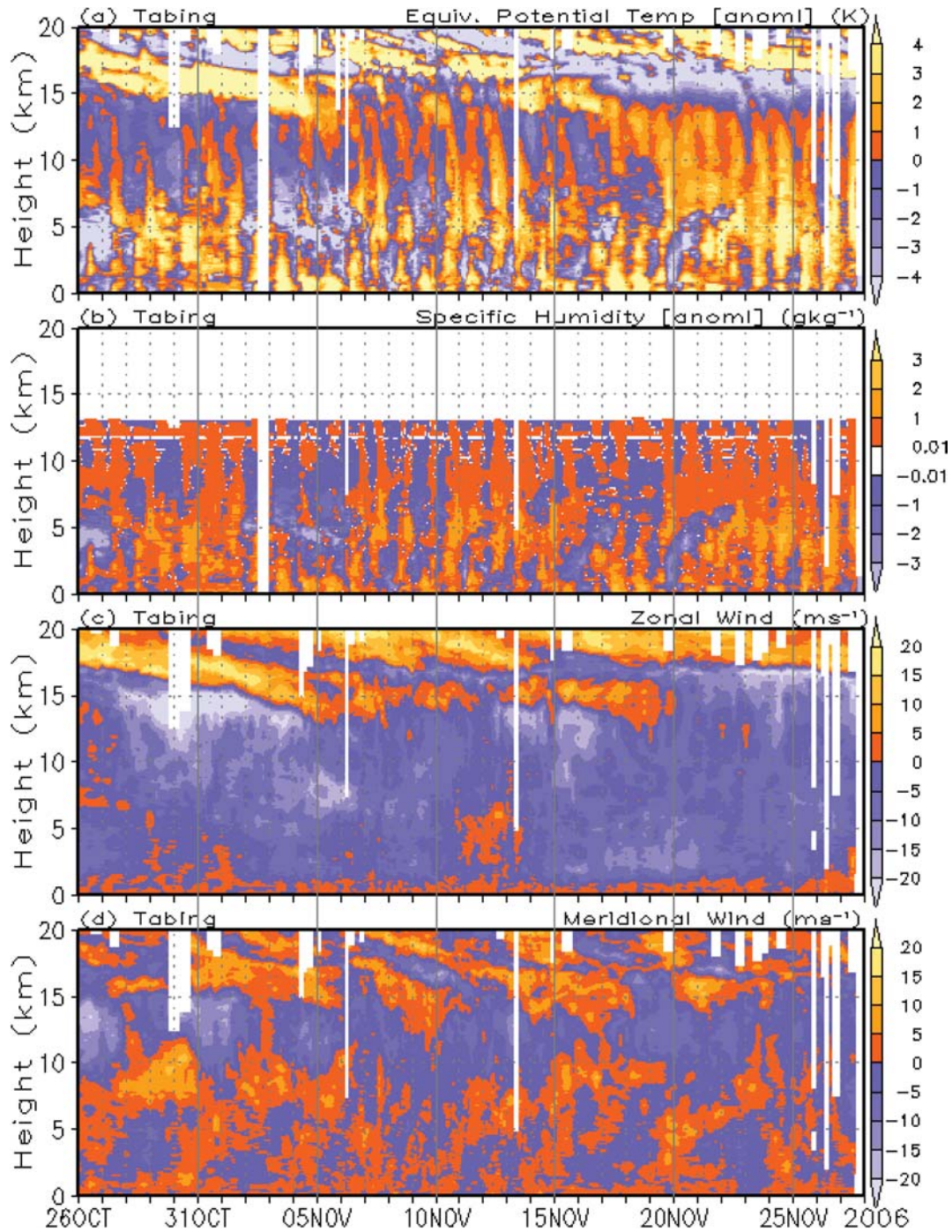


Fig. 5. Time-height cross-sectional views of equivalent potential temperature (a), specific humidity (b), and zonal (c) and meridional (d) wind velocity obtained by intensive soundings at Tabing from 26 October to 27 November 2006. Equivalent potential temperature and specific humidity are shown as anomalies from the period mean at each height.

Figure 6 shows time series of (a) surface pressure, (b) solar radiation, (c) specific humidity, (d) convective available potential energy (CAPE) and convective inhibition (CIN), and (e) area-averaged daily rainfall at 2 km AMSL during the campaign period. Data in (a), (b), and (c) were observed with the AWS installed at the MIA-XDR site. The CAPE and CIN were obtained from each sounding at Tabing. The area-averaged daily rainfall was calculated from MIA-XDR observations of every 6 min, and summed to reach the daily rainfall amount. The area-averaged rainfall (e) could be divided into three periods: 7–14 November (8 days), 22–27 November (6 days), and others, selecting series of rainy days which had daily rainfall amounts greater or less than the value of period averaged daily rainfall (2.9 mm day^{-1}). We hereafter refer to the former two periods as precipitation period (PP) 1 and 2.

As shown in Fig. 6, the daily average surface pressure (a) exhibited a decreasing trend during the entire period which corresponded to the approach of the large-scale disturbance; however it increased when the PP1 and PP2 events occurred. Specific humidity (c) also exhibited long-term variation, which showed a general increase before the PP1 and PP2 events started and then decreased gradually during the PPs. On the other hand, solar radiation reached a higher value during the PP1 and PP2 periods than on other non-PP days, even though its daily average did not show any specific variability.

The convective rain fraction (e) was almost double to the stratiform rain fraction in PP1. However, convective and stratiform rain fractions were almost the same in PP2. Although daily rainfall was slightly less than the period averaged rainfall amount, three days (28–30 October) at the beginning of the period could also be identified as a PP with considerable rainfall. Hence, all PPs in the beginning, middle, and end of entire period occurred when the zonal wind was weak easterly or westerly.

In addition, the daily average CAPE (d) was at a maximum just before PP1 and decreased during PP1. It again increased slightly after PP1, but decreased significantly when PP2 started. Although the CAPE showed variation with large values between the PPs, the CIN did not vary much during the whole period.

3.3 Coastal convective activities

a) Vertical profiles of echo area

Figures 7 and 8 show time-height cross sections of radar echo coverage obtained by the MIA-XDR

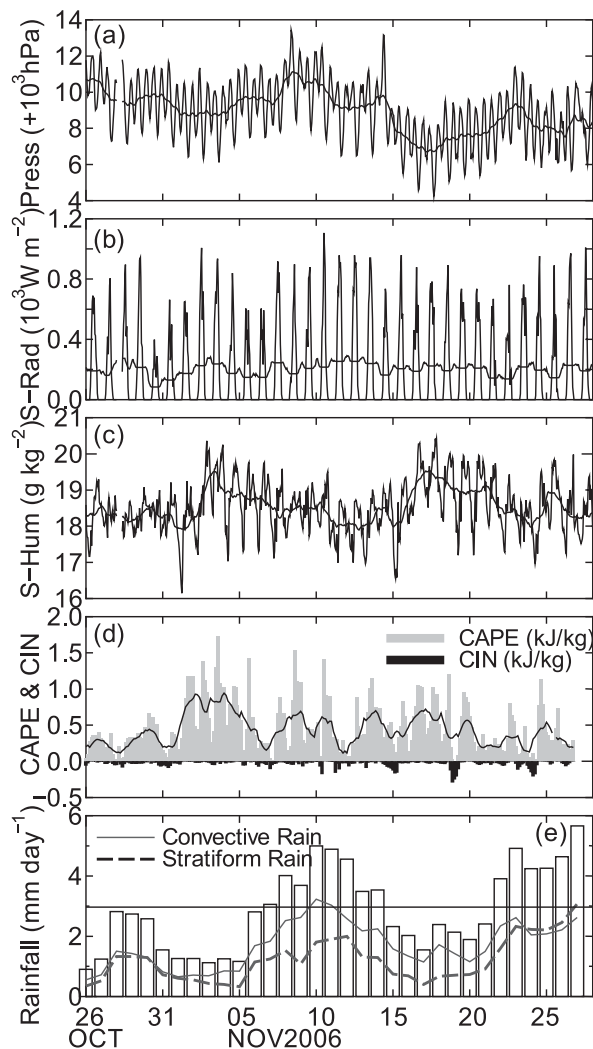


Fig. 6. Sequential variations in (a) surface pressure, (b) solar radiation, (c) specific humidity, (d) convective available potential energy (CAPE) and convective inhibition (CIN), and (e) area-averaged daily rainfall. The CAPE and CIN were calculated by each sounding at Tabing, and the daily area-averaged rainfall amounts at 2 km AMSL were observed with MIA-XDR. Other data were observed with the AWS at the MIA-XDR site during the HARI-MAU2006 campaign period. A black line in panel (d) indicates daily average value of CAPE. A horizontal line in panel (e) is the period mean of area-averaged rainfall of 2.97 mm day^{-1} . The thin solid and thick broken lines in panel (e) are convective and stratiform rain fractions, respectively.

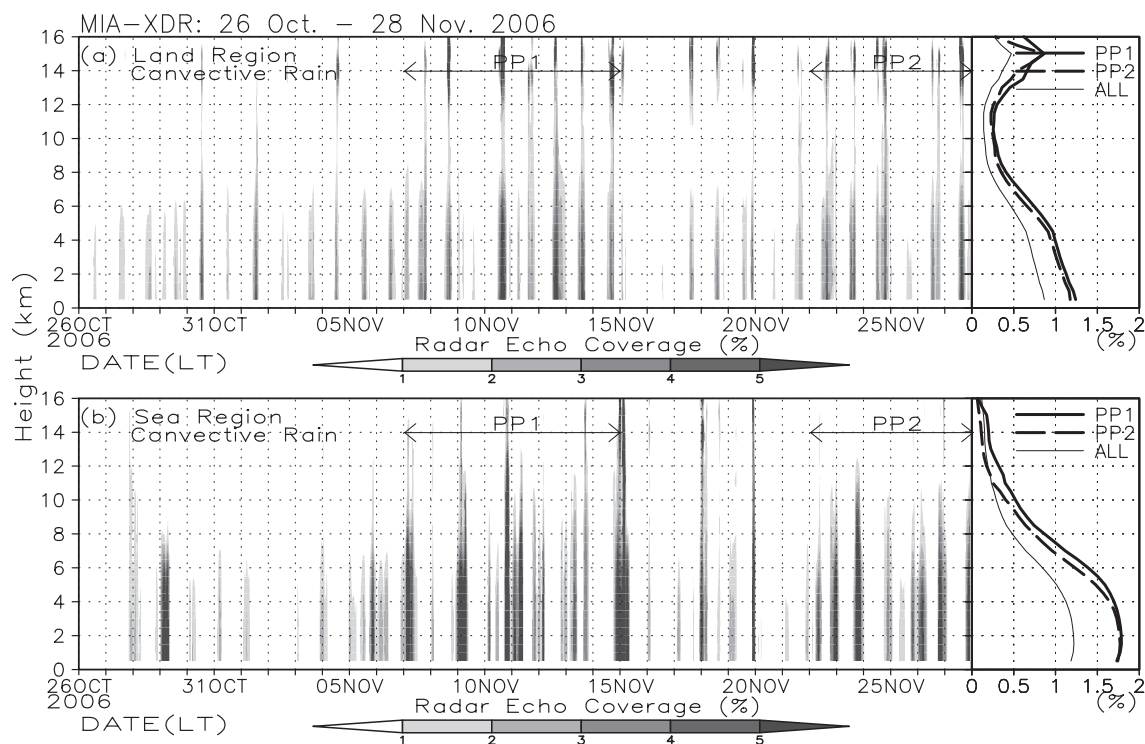


Fig. 7. Time-height cross sections of radar echo coverage observed with the MIA-XDR during the HARI-MAU2006 campaign period for convective rain type over land (a) and the sea (b) regions. The right-hand panels show the average profiles for PP1, PP2, and the whole period.

for each surface and rain type, along with the average profiles for PP1, PP2, and all periods on the right-hand side. The echo area of the convective rain was larger in both PP1 and PP2 over the sea (Fig. 7b) than over land (Fig. 7a), especially below 6 km AMSL. In addition, profiles of convective rain over land decreased significantly with height from the near surface to 10 km, but profiles over the sea exhibited nearly twice as much coverage as those over land from the near surface to 6 km AMSL. There were peaks of echo coverage around 2 km AMSL over the sea. Though values over land and the sea were larger in PP1 than in PP2, the difference between them was quite small over the entire height range.

On the other hand, areal coverage of stratiform rain echoes over the sea region (Fig. 8b) was much larger in PP2 than that in PP1. The difference became larger as the height decreased. Values over land (Fig. 8a) did not show much difference between PP1 and PP2, although they were a little larger in PP2 throughout the heights. Profiles of echo area peaked at higher altitudes (around 3 km

AMSL) over the sea than over land and decreased significantly near the surface.

These results indicate that the different characteristics of convective activities between PP1 and PP2, as illustrated in Fig. 6e were due to the changes in stratiform rather than convective rainfall, especially over the sea. In addition, the echo coverage of convective rainfall over the sea maintained larger area than that over land throughout both PP1 and PP2.

b) Diurnal variations

Figure 9 presents the diurnal variations in echo coverage at 2 km AMSL observed by the MIA-XDR for (a) convective rain over land, (b) stratiform rain over land, (c) convective rain over sea, and (d) stratiform rain over sea. The top and side panels in Fig. 9 (a)–(d) show variation in daily average and average diurnal variation, respectively, for PP1, PP2, and the entire period.

The echo coverage of convective rain over land (a) was at a maximum at 15 LT. It did not shift in local time much during the whole period. The max-

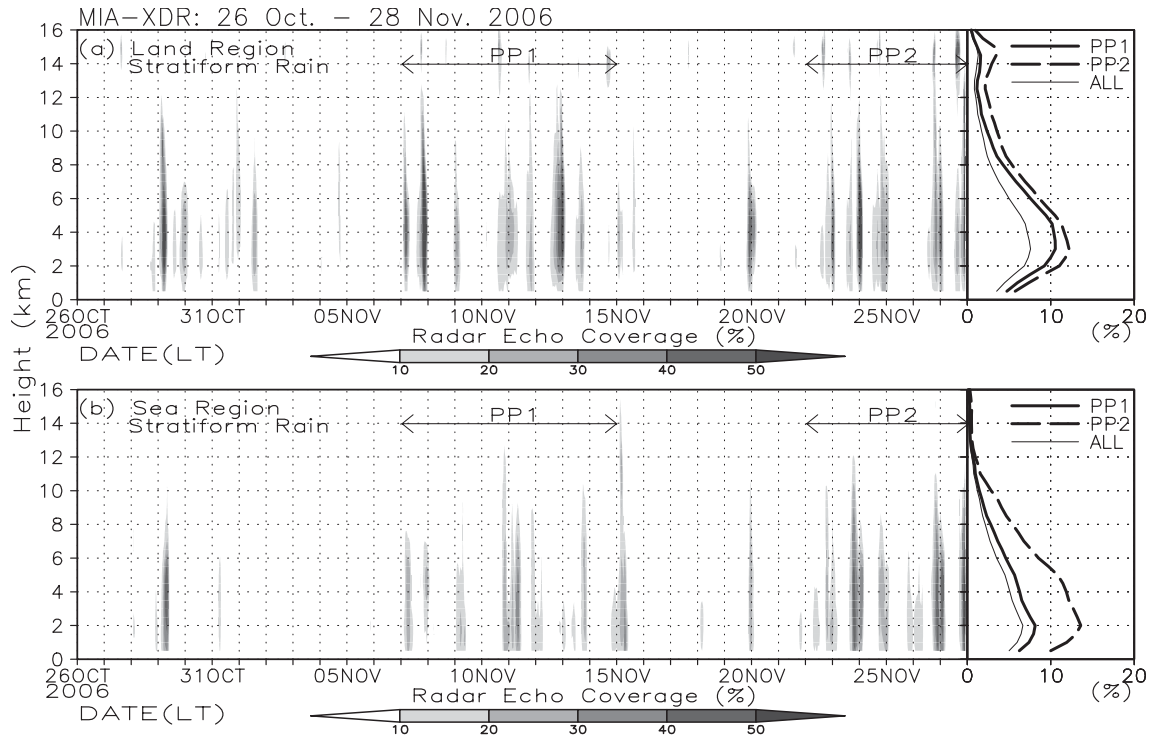


Fig. 8. Same as Fig. 7 but for stratiform rain type.

imum diurnal variation was larger in PP1 (4.3%) than in PP2 (3.7%) (side panel), although the daily average echo coverage did not differ by more than about 1.0–1.5% between PP1 and PP2 (top panel). However, the values over the sea (c) were completely different. The mean diurnal variation over the study period (side panel) had a gentle peak between late evening (21 LT) and early morning (04 LT) and a minimum at 14 LT. However, definite double-maximum peaks were seen at 20–21 LT in PP2 (4.8%) and 04 LT in PP1 (4.0%). The daily average echo coverage was larger in PP1 than in PP2, with a maximum of around 2.7% compared with 2.1% (top panel).

The echo coverage of the stratiform rain type over land (b) show a nocturnal flat maximum between 15 and 01 LT (approximately 20%) following the convective rain peak (a) and a minimum at 09 LT as its period mean (side panel). The nocturnal peak in PP2 (23–01 LT) was sharp, while the daily average echo coverage (top panel) did not differ greatly between PP1 and PP2 (around 10–20%). Values over the sea (d) showed similar DVs, with nocturnal maxima at 21–22 LT both in PP1 and PP2 and secondary maxima in early morning (01–

05 LT). However, the maximum peak in PP2 was larger (50%) than that in PP1 (24%). As a result, the daily average echo coverage (top panel) was much larger in PP2 (more than 20%) than in PP1 (less than 20%).

c) Diurnal migration of coastal convection

Figure 10 shows a Hovmöller diagram of radar reflectivity in the rectangle depicted in Fig. 1b, as observed by the MIA-XDR throughout the HARI-MAU2006. The reflectivity at 2 km AMSL was averaged over the short axis of the rectangle. A vertical solid line at 0 km in each panel, which marks the location of the MIA-XDR, roughly corresponds to the coastline of Sumatera Island. The rectangle was 160 km long, 20 km wide, and nearly perpendicular to the coastline. Convection was generated approximately 20–40 km inland from the coastline almost every day. Some convection cells migrated toward the offshore side (e.g., 29 October, 07 and 27 November). However, some other cells (e.g., those on 9, 11, and 15 November) developed offshore about 40–80 km from the coastline, independent of those over land. The frequency of the convective migration increased, especially in the

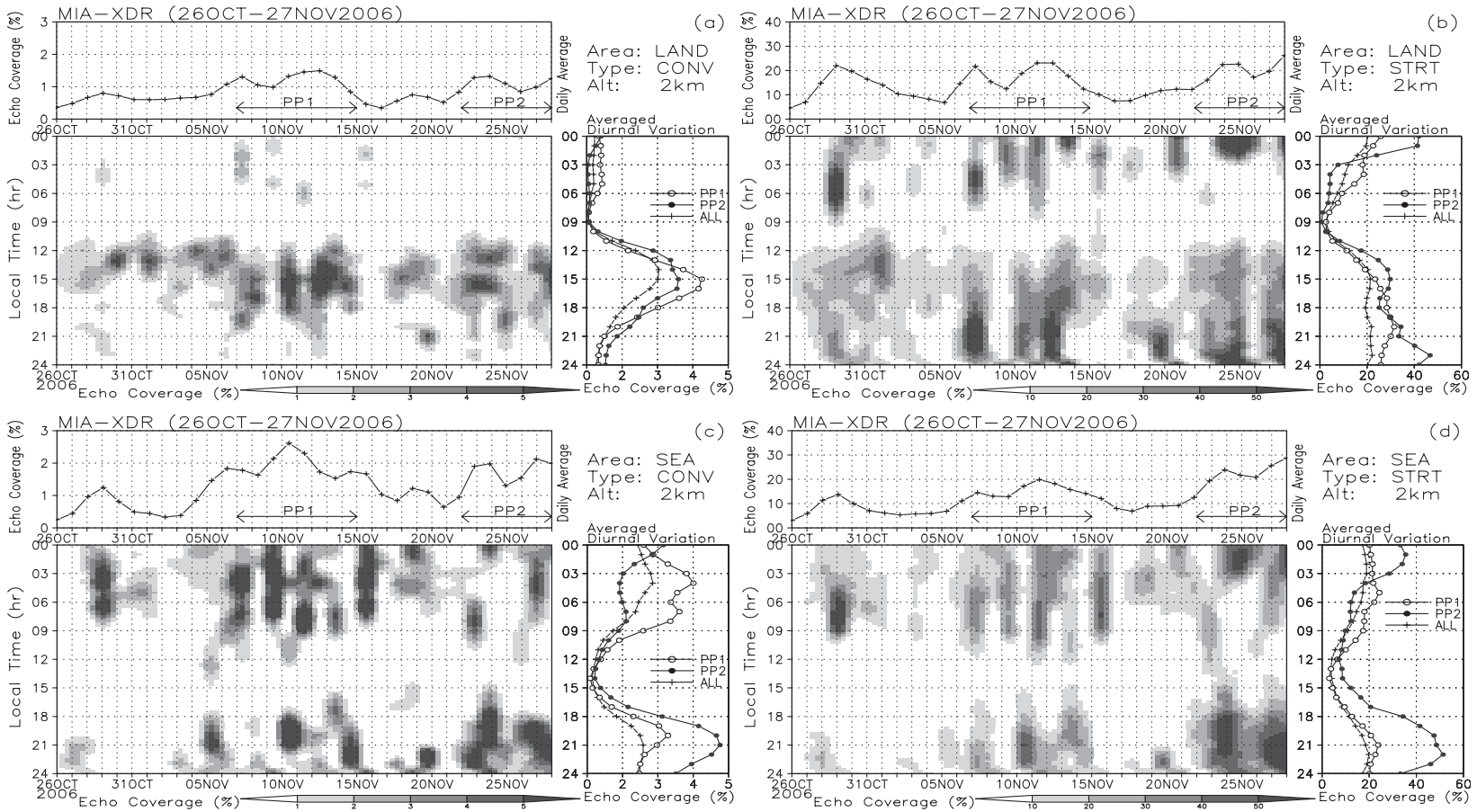


Fig. 9. Diurnal and periodic variations in echo coverage at 2 km AMSL observed with the MIA-XDR for (a) convective rain over land, (b) stratiform rain over land, (c) convective rain over the sea, and (d) stratiform rain over the sea. Top and side panels in (a)–(d) are the daily averaged variation and averaged diurnal variation for PPI, PP2, and the whole period, respectively.

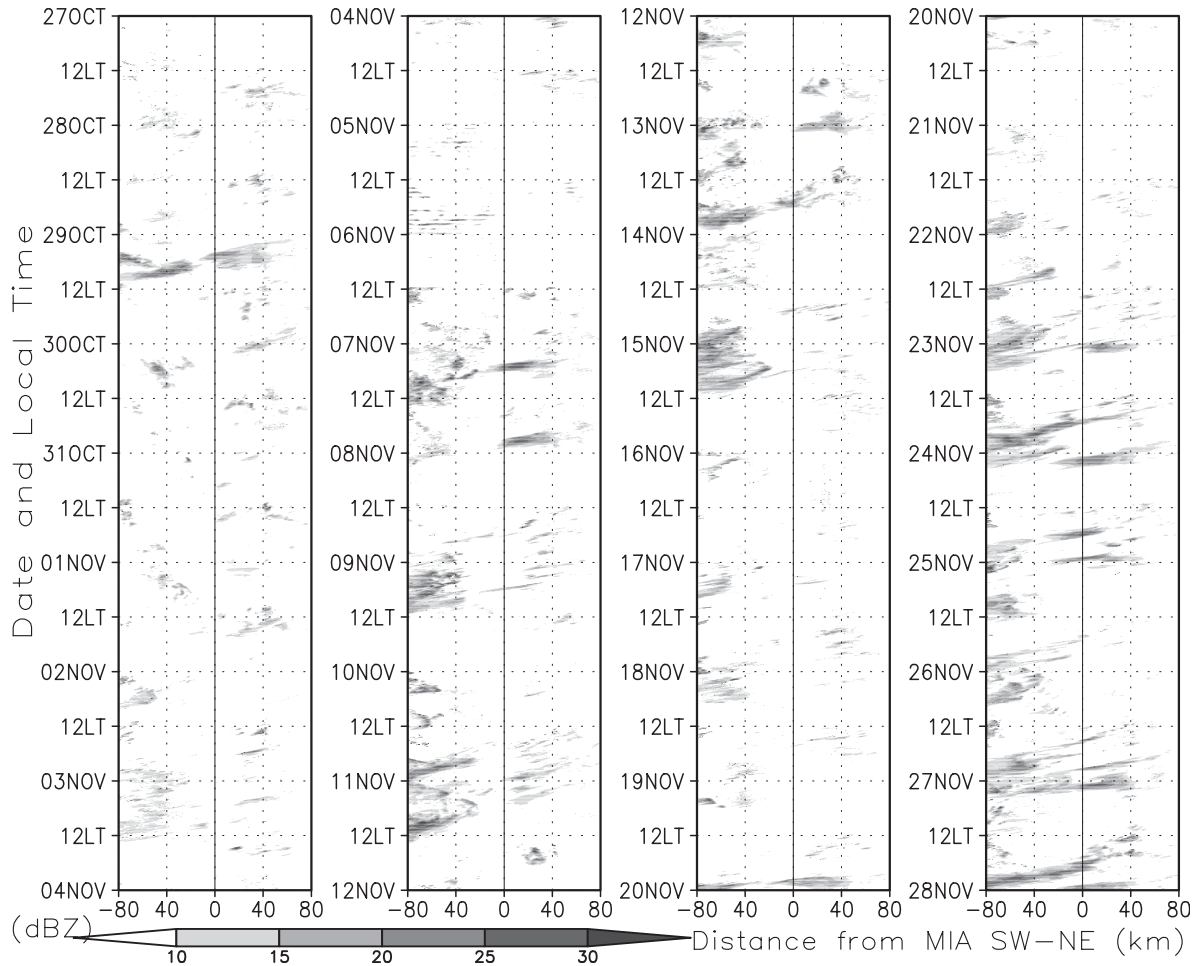


Fig. 10. Hovmöller diagram of radar reflectivity at 2 km AMSL in the rectangle depicted in Fig. 1b, observed with the MIA-XDR throughout the HARIMAU2006 campaign period. The reflectivity was averaged along the short axis of the rectangle. A vertical solid line at 0 km in each panel, which is the location of the MIA-XDR, roughly corresponds to the southwestern coastline of Sumatra Island.

last quarter of the campaign period, when the large-scale disturbance approached Sumatra Island.

Average diurnal variations in (a) radar reflectivity at 2 km AMSL, (b) rainfall intensity, (c) convective rain fraction, and (d) daily accumulated rainfall and topography along the rectangle are shown in Fig. 11. Convection was generated in the southwestern foothills of the mountain range in the early afternoon (12–15 LT). It developed until 18 LT at a similar position (Fig. 11a). Part of the convective system remained over the coastal land region and maintained weak reflectivity until the next morning. The other part migrated offshore at a speed of approximately 4 m s^{-1} (thick broken lines), before intensifying significantly around 21 LT about 40–

80 km from the coastline. The redeveloped convection maintained its position and strength throughout the night. Other convective cells developed 40–80 km offshore between 06 and 09 LT in the morning, independent of those over land. Consequently, the rainfall intensity (Fig. 11b) was high only in the afternoon to evening over the coastal land region. However, rainfall intensity over the coastal sea, on the other hand, showed two peaks: in the late evening and the following morning. As a result, there were double peaks of the daily rainfall maximum both over the coastal sea and land regions of approximately 3.5 mm, but the peak over the sea (land) was broad (narrow) and produced larger (smaller) amounts of rainfall (Fig. 11d). Al-

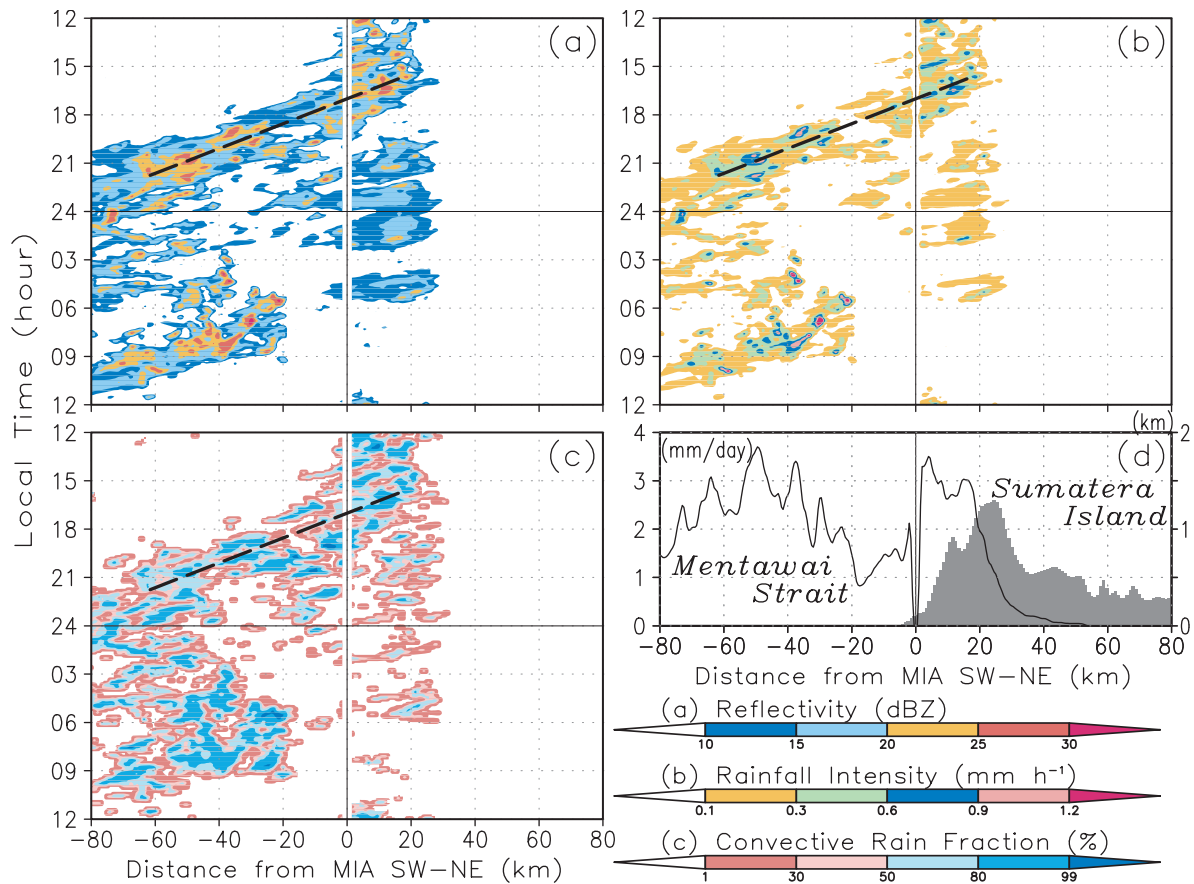


Fig. 11. Average diurnal variations in (a) radar reflectivity at 2 km AMSL, (b) rainfall intensity, (c) convective rain fraction, and (d) accumulated daily rainfall amount and topography along the rectangle in Fig. 1b during the HARIMAU2006 campaign period. Thick broken lines in (a), (b), and (c) indicate migration speeds of approximately 4 m s^{-1} . A vertical solid line at 0 km in each panel, which is the location of the MIA-XDR, roughly corresponds to the southwestern coastline of Sumatera Island, as in Fig. 10.

though more than 50% of the rainfall came from convective clouds in only 6 hours (12–18 LT) over the coastal land region followed by rainfall with a smaller fraction rate ($<50\%$), rainfall over the coastal sea region consisted of a convective fraction ($>50\%$) that was maintained more than 12 hours (21–09 LT) through the night to the next morning (Fig. 11c).

Figure 12 shows averaged vertical profiles of wind speed along the rectangle (i.e., perpendicular to the coastline; positive value for the southwesterly wind) every 3 hours as observed by soundings at Taging and a hodograph at 100 m AMSL. These wind profiles can be partitioned into three height regions: 1) northeasterly trade winds above 1.5 km, 2) southwesterly monsoonal wind at 0.5–1.5 km, and 3) land-sea breeze circulation below

0.5 km. The land-sea breeze circulation was dominant around 100 m AMSL, as shown in the hodograph. The sea breeze in the daytime helped to generate new convection over the coastal land region by local convergence at the foothills of the mountain range. The land breeze during the night created favorable conditions for new convection over the coastal sea region by converging with the synoptic southwesterly wind, though it was weak and shallow below 1 km AMSL (also see Fig. 5d and 5e). Although these convergences were not strong, atmospheric instability during the period was enough for convective genesis (Fig. 6). Furthermore, large vertical wind shears (roughly $5 \text{ m s}^{-1} \text{ km}^{-1}$ at 1–2 km) were fundamental factors for maintaining the long-lasting nocturnal convection over the coastal sea (Ogura and Yoshizaki 1988). Because

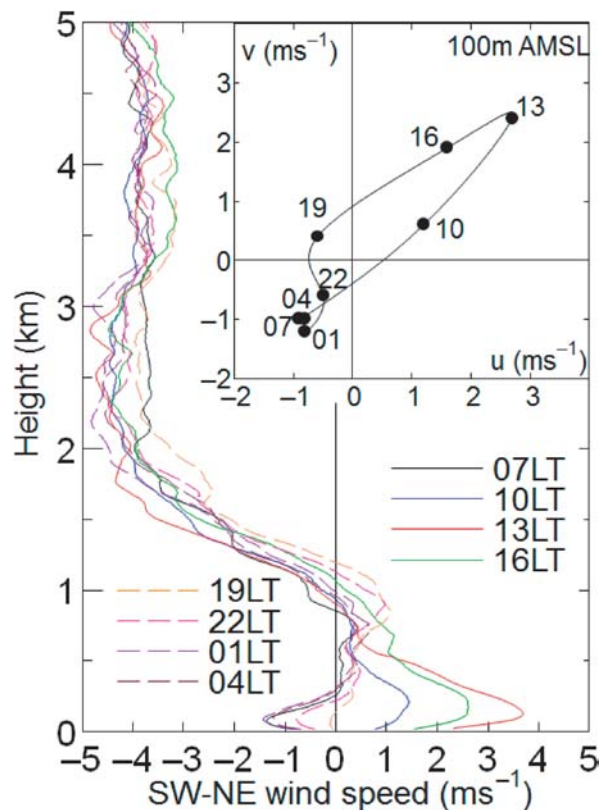


Fig. 12. Average vertical profiles of wind speed along the rectangle in Fig. 1b (i.e., perpendicular to the coastline; positive value for southwesterly wind) observed at Taping every 3 or 6 hours during the HARIMAU2006 campaign period, and a hodograph at 100 m AMSL.

the wind speed of convective migration in the evening corresponded to that of northeasterly trade wind above 2 km, convection seemed to be advected by the synoptic ambient wind on average.

4. Discussion

4.1 Different characteristics of convection in PP1 and PP2, and over land and sea

In this subsection, we examine the different characteristics of convection observed in our study between PP1 and PP2, and over the coastal land and sea regions. We then compare the results with those for convection over the inland region of Sumatera Island and the coastal sea region of Borneo (Kalimantan) Island of the IMC.

Because the large-scale disturbance was identified as an ISV that passed over the MIA-XDR site after 17 November as shown in Fig. 2, we can presume

that PP1 (PP2) was in an ISV inactive (active) phase. Major differences in convective activity between PP1 and PP2, and between land and sea, are summarized below:

- 1) The convective rain fraction in PP1 was nearly twice the stratiform rain fraction. On the other hand, the rain fractions in PP2 were almost equal, as shown in Fig. 6e.
- 2) The vertical profiles of echo coverage for convective rain were similar in PP1 and PP2 (although slightly larger in PP1), both over land and sea (Fig. 7), whereas the vertical profile for stratiform rain in PP2 was larger than that in PP1, especially in the lower troposphere over the sea (Fig. 8).
- 3) Although the echo coverage of convective rain over land decreased rapidly with height from the near surface to 10 km AMSL, that over the sea maintained almost twice the echo coverage of that over land from the near surface to 6 km AMSL both in PP1 and PP2 (Fig. 7).
- 4) The nocturnal rainfall peaks were larger in PP2 than those in PP1 in all cases except for convective rain over land. Rainfall peaks in PP1 were larger only for convective rain in the afternoon over land and early morning over the sea (Fig. 9).

As shown in Fig. 6, the CAPE during the campaign period was largest just before PP1 and then decreased until PP2 started. It seems that the convection associated with the large convective rain fraction in PP1 required high instability to be generated, which it then consumed by creating much rainfall. The southwesterly wind in the lower troposphere observed during PP1 (Fig. 5c and 5d) also formed favorable conditions for the generation of local convection along the coastline, by convergence with the northeasterly land breeze at night (Fig. 12). However, convection composed equally of both convective and stratiform rain in PP2 did not require such local instability because the large-scale disturbance of ISV supplied heat energy and water vapor (Fig. 5a and 5b) from the Indian Ocean, although easterly wind was dominant in the middle troposphere over Sumatera Island during this period.

These differences in convection between in PP2 (ISV active) and PP1 (ISV inactive) are consistent in general with the results of Kawashima et al. (2006) who studied convective activity during the MJO active and inactive phases using XDR data

from west Sumatera Island. However, their data covered only the inland region and did not include the major rainy season. Our results show that the greatest differences between PP1 and PP2 came from convective activity, especially its stratiform fraction, over the sea rather than over the land, as shown in Figs. 7, 8, and 9. In addition, the convective rain over the coastal sea region first peaked at around 21 LT (Fig. 9c), almost at the same time as the stratiform peak (Fig. 9d). Over land, the peak in echo coverage of convective rain at around 15 LT (Fig. 9a) was followed by a gentle increase in stratiform rain during the late evening to nighttime (Fig. 9b), as described by Kawashima et al. (2006). The characteristics of diurnal variation over the sea (Fig. 9c and 9d) were also different from those for a typical lifecycle of MCS evolution in the tropical open oceans (Houze 1982). It is possible that the nocturnal maximum of stratiform fraction over the coastal sea region comprised a combination of offshore-generated convection and convection advected from over land, which reached its secondary maximum in the evening. However, we need more case studies to examine this process in greater detail.

Houze et al. (1981) analyzed convective activity over the northwestern coastal sea region of Borneo (Kalimantan) Island based on observations with a C-band radar during the boreal winter monsoon season. Their results showed clear peaks of total radar echo coverage at 23 LT and 08 LT over coastal land and sea regions, respectively. This result differed from our findings, which showed a double peak time of radar echo coverage for both convective and stratiform rain over the coastal sea region especially in PP1 and PP2. The peak at around 21 LT, in particular, was not seen in Houze et al.'s (1981) study. The diurnal variation over the coastal sea region in our study with a double peak time may have been caused by diurnal land-sea migration of convection over the southwestern coastline of Sumatera Island (Mori et al. 2004; Sakurai et al. 2005). This is discussed more in the next subsection. Ichikawa and Yasunari (2006) found that although there was similar migration of convection over the northwestern side of Borneo (Kalimantan), the rainfall over the coastal sea region that, Houze et al. (1981) studied, peaked in the early morning because it was not disturbed by diurnal convective migration from the coastal land because of the Borneo vortex. Therefore, it is a unique mechanism to maintain the DV in convection over the northwest-

ern coastal sea of Borneo (Kalimantan) Island and cannot explain the convective characteristics over the southwestern coastline of Sumatera Island.

4.2 Coastal heavy rainbands

Previous studies revealed the CHeR along the southwestern coastline of Sumatera Island after the era of the TRMM satellite (Mori et al. 2004; Sakurai et al. 2005; Sakurai et al. 2009; Wu et al. 2009). Xie et al. (2006) found similar CHeRs are commonly observed over the Asian monsoon region, such as the Indian coast west of the Western Ghats, the western coast of Myanmar over the Bay of Bengal and the Andaman Sea, northeastern coast of the Gulf of Thailand, the eastern coast of Vietnam, and the northwestern Philippines. On the basis of their analysis of the boreal summer monsoon season (June, July, August), they suggested that most of these CHeRs could be generated by interaction between the southwesterly monsoon flow and orographic convergence along the coastlines (wind-terrain interaction). On the other hand, the CHeR along Sumatera Island was seen throughout the year, even though easterly wind was dominant in the lower troposphere. Indeed, the offshore peak of daily rainfall was clearly observed in our study (Fig. 11d) as well as a comparable peak in the foothills of the mountain range. Rainfall intensity during this period (Fig. 6e) was not enough to produce the climatological CHeR (more than $3,000 \text{ mm y}^{-1}$) shown in Fig. 1a because our observational period was mainly in the convectively ISV inactive phase.

The CHeR along the Indian coast near the Western Ghats, which has a rainfall peak over the coastal ocean rather than in the foothills, was studied by Ogura and Yoshizaki (1988) by using an idealized numerical simulation. They found that two factors were essential to generate the CHeR: 1) heat and moisture fluxes supplied from the coastal ocean, and 2) vertical wind shear between the southwesterly monsoon flow in the lower levels and the easterly wind layer above. The environmental wind profiles in our case (Fig. 12) satisfied at least the second requirement. However, the southwesterly wind flow was not stronger during the campaign period than its climatology (Okamoto et al. 2003) because it occurred in the convectively inactive ISV phase.

Although Ogura and Yoshizaki (1988) did not examine the diurnal variation in coastal convection, our study (Fig. 11) clearly showed that it must also be essential to generate the CHeR along Sumatera

Island. As shown in Fig. 11, convection was generated in the foothills of the mountain range in the early afternoon. One part of the convective system was maintained there with weak reflectivity and a smaller convective rain fraction throughout the night. Another part of the convective system migrated into the offshore region at a speed of approximately 4 m s^{-1} and then redeveloped at around 21 LT about 40–80 km off the coastline. Furthermore, more offshore convection developed independently at around 06–09 LT about 20–80 km off the coastline, corresponding to the morning rainfall peak also observed in the northwestern coastal sea region of Borneo (Kalimantan) Island (Houze et al. 1981). Sakurai et al. (2009b) examined the interaction between convection from the coastal land and that generated over coastal sea, and then found that this interaction enhanced the coastal rainfall though they examined only one day case.

All these results suggest that the CHeR along the Sumatra Island is formed by diurnally developed coastal convection composed of two major parts: 1) migration of convection from the coastal land and its redevelopment in the late evening, and 2) independent generation of convection over the coastal sea region in the early morning. In addition, we speculate that specific interaction mechanisms, such as the seeder-feeder process between 1) and 2) (Mori et al. 2004), may enhance the CHeR. Moreover, because the Mentawai Strait is shallow and mostly separated from the Indian Ocean by an archipelago along Sumatra Island as shown in Fig. 1b, a high sea surface temperature (SST) must be formed easily in the daytime if the winds are not strong. Hence, it is possible that a large amount of heat and moisture fluxes from the sea surface of the Mentawai Strait enhance the CHeR as Ogura and Yoshizaki (1988) concluded.

5. Concluding remarks

This paper presented an overview of convective activity during the HARIMAU2006 campaign, focusing on the differences between coastal land/sea and inactive/active ISV phases based on observations from the XDR and intensive soundings at Sumatra Island. In addition, the DV in coastal convection and formation of CHeR were also examined in terms of the diurnal land-sea migration of coastal convective systems.

Although the campaign period corresponded to the major rainy season over Sumatra Island, the ISV phase was inactive during the beginning and

middle of the observation period. However, the phase became active near the end of period. We defined the two major precipitation periods of PP1 and PP2 as the ISV inactive and active phases, respectively. PP1 contained convective rain fractions nearly twice that of the stratiform rain fractions, but PP2 was composed of both rain fractions almost equally.

The vertical profiles of echo coverage for convective rain were similar in PP1 and PP2 over both the coastal land and the adjacent offshore region. The vertical profile for stratiform rain in PP2 had greater coverage than that in PP1, especially in the lower troposphere over the sea. Although the echo coverage of convective rain over land decreased rapidly with height from the near surface to 10 km AMSL, the convective echo profiles over the sea exhibited nearly twice as much coverage as those over land from the near surface to 6 km AMSL, both in PP1 and PP2. The nocturnal rainfall maxima were larger in PP2 than in PP1 in all cases except for convective rain over land. Rainfall maxima during PP1 were larger only for convective rain in the afternoon over land and early morning over the adjacent sea.

Highly unstable environmental conditions were responsible for the convection in PP1, which instability was then consumed by creating significant amounts of rainfall. The southwesterly wind flow in the lower troposphere observed during PP1 also led to favorable conditions for the generation of local convection along the coastline due to convergence with the northeasterly land breeze at night. However, that in PP2 was formed due to the large-scale disturbance of ISV, which supplied heat energy and water vapor from the Indian Ocean.

Convection was generated in the southwestern foothills of the mountain range in the early afternoon (12–15 LT). It continued growing until 18 LT at a similar position. Part of the convective system remained over the coastal land region and maintained weak reflectivity until the next morning. The other part migrated offshore at a speed of approximately 4 m s^{-1} , before intensifying significantly around 21 LT in the offshore region. However, other convective cells developed offshore in the early morning independent of those over the land. As a result, double maxima of the daily rainfall were observed both over the coastal sea and land, but the maximum over the sea (land) was broad (narrow) and produced a larger (smaller) amount of rainfall.

All these results suggest that the CHeR along Sumatera Island is formed by diurnally developed coastal convection composed of two major parts: 1) migration of convection from the coastal land and its redevelopment in the late evening, and 2) independent generation of convection over the coastal sea region in the early morning. In addition, we speculate that specific interaction mechanisms, such as the seeder-feeder process between 1) and 2) and/or the abundant heat and moisture fluxes supplied from the Mentawai Strait between the islands of Sumatera and Siberut may enhance the CHeR. However, open questions remain. It is important to proceed to highly detailed studies of individual cases to determine how the CHeRs are formed as a next step in employing dual XDR analysis, numerical model simulation, coastal ocean flux monitoring, and newly introduced dual-polarimetric radar observations.

Acknowledgements

The HARIMAU project, led by Japan Earth Observing System (EOS) Promotion Program (JEPP) of the Ministry of Education, Culture, Sports, Science and Technology (MEXT) of Japan, has been operated based on collaboration between the BPPT (Agency for the Assessment and Application of Technology), BMKG (Meteorology, Climatology, and Geophysical Agency), and LAPAN (National Institute of Aeronautics and Space) on the Indonesian side, and JAMSTEC, Hokkaido University, and Kyoto University on the Japanese side. The authors express their thanks to Professor Yasushi Fujiyoshi and Mr. Masayuki Ohi of Hokkaido University for coordinating and technically supporting the X-band Doppler radar observations at Tiku and MIA. The authors express their thanks to Drs. Masaki Katsumata and Hisayuki Kubota of JAMSTEC, and Taro Shinoda of Nagoya University for their helpful discussions and positive comments. Thanks are also extended to two anonymous reviewers, whose constructive comments greatly improved the content of this manuscript.

References

- Fukao, S., 2006: Coupling processes in the equatorial atmosphere (CPEA): A project overview. *J. Meteor. Soc. Japan*, **84A**, 1–18.
- Fudeyasu, H., K. Ichianagi, K. Yoshimura, S. Mori, N. Sakurai, J.-I. Hamada, M. D. Yamanaka, J. Matsumoto, and F. Syamsudin, 2011: Effects of large-scale moisture transport and mesoscale processes on precipitation isotope ratios observed at Sumatera, Indonesia. *J. Meteor. Soc. Japan*, **89A**, 49–59.
- Hamada, J.-I., M. D. Yamanaka, J. Matsumoto, S. Fukao, P. A. Winarso, and T. Sribimawati, 2002: Spatial and temporal variations of the rainy season over Indonesia and their link to ENSO. *J. Meteor. Soc. Japan*, **80**, 285–310.
- Hamada, J.-I., M. D. Yamanaka, S. Mori, Y. I. Tauhid, and T. Sribimawati, 2008: Differences of rainfall characteristics between coastal and interior areas of central western Sumatera, Indonesia. *J. Meteor. Soc. Japan*, **86**, 593–611.
- Hara, M., T. Yoshikane, H. G. Takahashi, F. Kimura, A. Noda, and T. Tokioka, 2009: Assessment of the diurnal cycle of precipitation over the maritime continent simulated by a 20 km Mesh GCM using TRMM PR Data. *J. Meteor. Soc. Japan*, **87A**, 413–424.
- Hirose, M., and K. Nakamura, 2005: Spatial and diurnal variation of precipitation systems over Asia observed by the TRMM Precipitation Radar. *J. Geophys. Res.*, **110**, D05106, doi:10.1029/2004JD004815.
- Hirose, M., R. Oki, S. Shimizu, M. Kachi, and T. Higashiwatoko, 2008: Finescale diurnal rainfall statistics refined from eight years of TRMM PR data. *J. Appl. Meteor. Climat.*, **47**, 544–561.
- Houze, R. A., Jr., 1982: Cloud clusters and large-scale vertical motions in the tropics. *J. Meteor. Soc. Japan*, **60**, 396–410.
- Houze, R. A., Jr., S. G. Geotis, F. D. Marks, Jr., and A. K. West, 1981: Winter monsoon convection in the vicinity of north Borneo. Part I: Structure and time variation of the clouds and precipitation. *Mon. Wea. Rev.*, **109**, 1595–1614.
- Ichikawa, H., and T. Yasunari, 2008: Intraseasonal variability in diurnal rainfall over New Guinea and the surrounding oceans during Austral summer. *J. Climate*, **21**, 2852–2868.
- Johnson, R. H., P. E. Ciesielski, and J. A. Cotturone, 2001: Multiscale variability of the atmospheric mixed layer over the Western Pacific warm pool. *J. Atmos. Sci.*, **58**, 2729–2750.
- Kawashima, M., Y. Fujiyoshi, M. Ohi, T. Honda, T. Kozu, T. Shimomai, and H. Hashiguchi, 2006: Overview of Doppler radar observations of precipitating cloud systems in Sumatera island during the first CPEA campaign. *J. Meteor. Soc. Japan*, **84A**, 33–56.
- Kawashima, M., Y. Fujiyoshi, M. Ohi, T. Honda, S. Mori, N. Sakurai, Y. Abe, W. Harjupa, F. Syamsudin, and M. D. Yamanaka, 2011: Case study of an intense wind event associated with a mesoscale convective system in west Sumatera during the HARIMAU2006 campaign. *J. Meteor. Soc. Japan*, **89A**, 239–257.

- Kubota, H., and T. Nitta, 2001: Diurnal variations of tropical convection observed during the TOGA-COARE. *J. Meteor. Soc. Japan*, **79**, 815–830.
- Madden, R. A., and P. R. Julian, 1971: Detection of a 40–50 day oscillation in the zonal wind in the tropical Pacific. *J. Atmos. Sci.*, **28**, 702–708.
- Madden, R. A., and P. R. Julian, 1972: Description of global-scale circulation cells in the tropics with a 40–50 day period. *J. Atmos. Sci.*, **29**, 1109–1123.
- Mapes, B. E., T. T. Warner, M. Xu, and A. J. Negri, 2003: Diurnal patterns of rainfall in northwestern South America. Part I: Observations and context. *Mon. Wea. Rev.*, **131**, 799–812.
- Matsumoto, J., 1992: The seasonal changes in Asian and Australian monsoon region. *J. Meteor. Soc. Japan*, **70**, 257–273.
- Mori, S., J.-I. Hamada, Y. I. Tauhid, M. D. Yamanaka, N. Okamoto, F. Murata, N. Sakurai, H. Hashiguchi, and T. Sribimawati, 2004: Diurnal land-sea rainfall peak migration over Sumatera Island, Indonesian maritime continent observed by TRMM satellite and intensive rawinsonde soundings. *Mon. Wea. Rev.*, **132**, 2021–2039.
- Mori, S., J.-I. Hamada, M. D. Yamanaka, Y.-M. Kodama, M. Kawashima, T. Shimomai, Y. Shibagaki, H. Hashiguchi, and T. Sribimawati, 2006: Vertical wind characteristics in precipitating cloud systems over west Sumatera, Indonesia, observed with equatorial atmosphere radar: Case study of 23–24 April 2004 during the first CPEA campaign period. *J. Meteor. Soc. Japan*, **84A**, 113–131.
- Moteki, Q., R. Shirooka, H. Kubota, T. Ushiyama, K. K. Reddy, K. Yoneyama, M. Katsumata, N. Sato, K. Yasunaga, H. Yamada, B. Geng, M. Fujita, M. Yoshizaki, H. Uyeda, and T. Chuda, 2008: Mechanism of the northward propagation of mesoscale convective systems observed on 15 June 2005 during PALAU2005. *J. Geophys. Res.*, **113**, D14126, doi:10.1029/2008JD009793.
- Murakami, T., and J. Matsumoto, 1994: Summer monsoon over the Asian continent and western north Pacific. *J. Meteor. Soc. Japan*, **72**, 719–745.
- Neale, R., and J. Slingo, 2003: The maritime continent and its role in the global climate: A GCM study. *J. Climate*, **16**, 834–848.
- Nitta, T., T. Mizuno, and K. Takahashi, 1992: Multi-scale convective systems during the initial phase of the 1986/87 El Niño. *J. Meteor. Soc. Japan*, **70**, 447–466.
- Nitta, T., and S. Sekine, 1994: Diurnal variation of convective activity over the tropical western Pacific. *J. Meteor. Soc. Japan*, **72**, 627–641.
- Ogura, Y., and M. Yoshizaki, 1988: Numerical study of orographic-convective precipitation over the eastern Arabian Sea and the Ghat Mountains during the summer monsoon. *J. Atmos. Sci.*, **45**, 2097–2122.
- Ohsawa, T., H. Ueda, T. Hayashi, A. Watanabe, and J. Matsumoto, 2001: Diurnal variations of convective activity and rainfall in tropical Asia. *J. Meteor. Soc. Japan*, **79**, 333–352.
- Okamoto, N., M. D. Yamanaka, S.-Y. Ogino, H. Hashiguchi, N. Nishi, T. Sribimawati, and A. Numaguti, 2003: Seasonal variations of tropospheric wind over Indonesia: Comparison between collected operational rawinsonde data and NCEP reanalysis for 1992–99. *J. Meteor. Soc. Japan*, **81**, 829–850.
- Qian, J. H., 2008: Why precipitation is mostly concentrated over islands in the Maritime Continent. *J. Atmos. Sci.*, **65**, 1428–1441.
- Ramage, C. S., 1968: Role of a tropical “maritime continent” in the atmospheric circulation. *Mon. Wea. Rev.*, **96**, 365–369.
- Sakurai, N., F. Murata, M. D. Yamanaka, S. Mori, J.-I. Hamada, H. Hashiguchi, Y.-I. Tauhid, T. Sribimawati, and B. Suhardi, 2005: Diurnal cycle of cloud system migration over Sumatera Island. *J. Meteor. Soc. Japan*, **83**, 835–850.
- Sakurai, N., M. Kawashima, Y. Fujiyoshi, H. Hashiguchi, T. Shimomai, S. Mori, J.-I. Hamada, F. Murata, M. D. Yamanaka, Y. I. Tauhid, T. Sribimawati, and B. Suhardi, 2009a: Internal structures of migratory cloud systems with diurnal cycle over Sumatera Island during CPEA-I campaign. *J. Meteor. Soc. Japan*, **87**, 157–170.
- Sakurai, N., S. Mori, M. Kawashima, Y. Fujiyoshi, Hamada, J.-I., H. Fudeyasu, Y. Tabata, M. D. Yamanaka, J. Matsumoto, F. Syamsudin, and Emrizal, 2009b: Internal structure of westward migratory cloud systems with a diurnal cycle in west Sumatera observed on 10 November, 2006 during HARIMAU2006 campaign. *Proceedings of the international MAHASRI/HyARC workshop on Asian Monsoon*, 243–252, 5–7 March 2009, Da Nang, Vietnam.
- Schumacher, C., and R. A. Houze Jr., 2003: Stratiform rain in the tropics as seen by the TRMM precipitation radar. *J. Climate*, **16**, 1739–1756.
- Shibagaki, Y., T. Kozu, T. Shimomai, S. Mori, F. Murata, Y. Fujiyoshi, H. Hashiguchi, and S. Fukao, 2006: Evolution of a super cloud cluster and the associated wind fields observed over the Indonesian maritime continent during the first CPEA campaign. *J. Meteor. Soc. Japan*, **84A**, 19–31.
- Steiner, M., R. A. Houze Jr., and S. E. Yuter, 1995: Climatological characterization of three-dimensional storm structure from operational radar and rain gauge data. *J. Appl. Meteor.*, **34**, 1978–2007.
- Sui, C. H., X. Li, and K.-M. Lau, 1998: Radiative-convective processes in simulated diurnal variations of tropical oceanic convection. *J. Atmos. Sci.*, **55**, 2345–2357.
- Tanaka, M., 1994: The onset and retreat dates of the Austral summer monsoon over Indonesia, Australia.

- lia and New Guinea. *J. Meteor. Soc. Japan*, **72**, 255–267.
- Tao, W. K., S. Lang, J. Simpson, C. H. Sui, B. Ferrier, and M.-D. Chou, 1996: Mechanisms of cloud-radiation interaction in the tropics and midlatitude. *J. Atmos. Sci.*, **53**, 2624–2651.
- Wheeler, M., and K. M. Weickmann, 2001: Real-time monitoring and prediction of modes of coherent synoptic to intraseasonal tropical variability. *Mon. Wea. Rev.*, **129**, 2677–2694.
- Wu, P.-M., M. Hara, J.-I. Hamada, M. D. Yamanaka, and F. Kimura, 2009: Why a large amount of rain falls over the sea in the vicinity of western Sumatra Island during nighttime. *J. Appl. Meteor. Climat.*, **48**, 1345–1361.
- Xie, S. P., H. Xu, N. H. Saji, Y. Wang, and W. T. Liu, 2006: Role of narrow mountains in large-scale organization of Asian monsoon convection. *J. Climate*, **19**, 3420–3429.
- Yamanaka, M. D., S. Mori, P.-M. Wu, J.-I. Hamada, N. Sakurai, H. Hashiguchi, M. K. Yamamoto, Y. Shibagaki, M. Kawashima, Y. Fujiyoshi, T. Shimomai, T. Manik, Erlansyah, W. Setiawan, B. Tejasukmana, F. Syamsudin, Y. S. Djajadihardia, and J. T. Anggadiredja, 2008: HARIMAU radar-profiler network over Indonesian maritime continent: A GEOSS early achievement for hydrological cycle and disaster prevention. *J. Disaster Res.*, **3**, 78–88.
- Yang, G.-Y., and J. Slingo, 2001: The diurnal cycle in the tropics. *Mon. Wea. Rev.*, **129**, 784–801.
- Yasunari, T., 1981: Structure of an Indian summer monsoon system with around 40-day period. *J. Meteor. Soc. Japan*, **59**, 336–354.
- Yoneyama, K., M. Katsumata, K. Mizuno, M. Yoshizaki, R. Shirooka, K. Yasunaga, H. Yamada, N. Sato, T. Ushiyama, Q. Moteki, A. Seiki, M. Fujita, K. Ando, H. Hase, I. Ueki, T. Horii, Y. Masumoto, Y. Kuroda, Y. N. Takayabu, A. Shareef, Y. Fujiyoshi, M. J. McPhaden, V. S. N. Murty, C. Yokoyama, and T. Miyakawa, 2008: MISMO field experiment in the equatorial Indian Ocean. *Bull. Amer. Meteor. Soc.*, **89**, 1889–1903.
- Zhou, L., and Y. Wang, 2006: Tropical Rainfall Measuring Mission observation and regional model study of precipitation diurnal cycle in the New Guinean region. *J. Geophys. Res.*, **111**, D17104. doi:10.1029/2006JD007243.
- Zuidema, P., 2003: Convective clouds over the Bay of Bengal. *Mon. Wea. Rev.*, **131**, 780–798.